AJR FOCUS ON:

Practical Guide to Evaluating Myocardial Disease by Cardiac MRI

Elizabeth Lee[1]
El-Sayed H. Ibrahim[2]
Purvi Parwani[3]
Nicole Bhave[4]
Jadranka Stojanovska[1]

[1]Department of Radiology, Division of Cardiothoracic Radiology, University of Michigan, 1500 E Medical Center Dr, CVC Rm 5481, Ann Arbor, MI 48109-5868. Address correspondence to J. Stojanovska (jstoanov@med.umich.edu).

[2]Center for Imaging Research, Medical College of Wisconsin, Milwaukee, WI.

[3]Department of Medicine, Division of Cardiology, Loma Linda University Health, Loma Linda, CA.

[4]Department of Medicine, Division of Cardiology, University of Michigan, Ann Arbor, MI.

OBJECTIVE. A spectrum of pathophysiologic mechanisms can lead to the development of myocardial disorders including ischemia, genetic abnormalities, and systemic disorders. Cardiac MRI identifies different myocardial disorders, provides prognostic information, and directs therapy. In comparison with other imaging modalities, cardiac MRI has the advantage of allowing both functional assessment and tissues characterization in a single examination without the use of ionizing radiation. Newer cardiac MRI techniques including mapping can provide additional information about myocardial disease that may not be detected using conventional techniques. Emerging techniques including MR spectroscopy and finger printing will likely change the way we understand the pathophysiology mechanisms of the wide array of myocardial disorders.

CONCLUSION. Imaging of myocardial disorders encompasses a large variety of conditions including both ischemic and nonischemic diseases. Cardiac MRI sequences, such as balanced steady-state free precession and late gadolinium enhancement, play a critical role in establishing diagnosis, determining prognosis, and guiding therapeutic management. Additional sequences—including perfusion imaging, T2*, real-time cine, and T2-weighted sequences—should be performed in specific clinical scenarios. There is emerging evidence for the use of mapping in imaging of myocardial disease. Multiple other new techniques are currently being studied. These novel techniques will likely change the way myocardial disorders are understood and diagnosed in the near future.

Myocardial disease is broadly divided into ischemic and nonischemic. Many systemic disorders, genetic conditions, and adaptive states can lead to nonischemic cardiomyopathy (NICM). Imaging plays a critical role in the diagnosis of myocardial disease and risk stratification. Furthermore, the presence of imaging findings, such as late gadolinium enhancement (LGE), can provide prognostic information including the risk of adverse cardiac events and can also be used to determine therapeutic strategies such as revascularization in patients with ischemic cardiomyopathy (ICM) or ablation of arrhythmogenic foci in patients with ventricular arrhythmias. On the basis of the presence and distribution of LGE, it is possible to differentiate ICM from NICM. Cardiac MRI is the only imaging modality that allows precise assessment of ventricular function and comprehensive tissue characterization in a single examination without the use of ionizing radiation. Cardiac MRI also has the advantage of answering clinical questions to guide clinical management (Fig. 1).

Cardiac myocardial imaging is feasible at both 1.5 and 3 T, with higher-field-strength imaging in the domain of research. At 3 T, the signal-to-noise ratio (SNR) is improved compared with the SNR at 1.5 T, but this improvement is at the cost of worsening susceptibility artifact; a higher specific absorption rate; and an increase in B1 inhomogeneity, which predominately affects T2-weighted imaging [1]. Balanced steady-state free precession (bSSFP) imaging, a mainstay of cardiac MRI, is more prone to artifact at 3 T [2]. However, specific cardiac MRI sequences including myocardial tagging, spectroscopy, arterial spin labeling (ASL), and first-pass perfusion are improved at 3 T because T1 values are increased when using this field strength [3]. This increase in T1 values also improves contrast-enhanced imaging in cardiac MRI because the difference between T1 values of unenhanced and enhanced structures is larger [4].
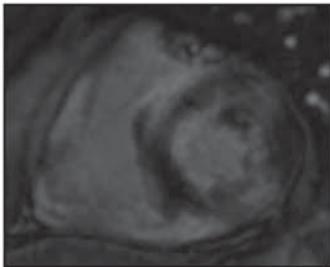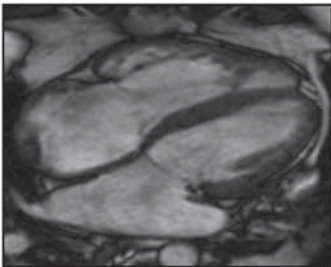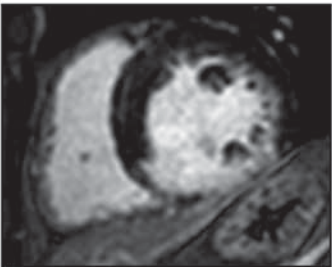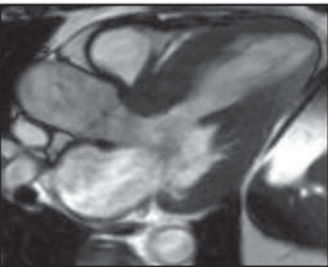
Fig. 1—Schematic lists tailored cardiac MRI pulse sequences that can be used to answer most common clinical questions from referring physicians. Left MR image is 45-year-old man with cardiac sarcoid; middle-left MR image is 56-year-old woman with cardiac arrhythmia; middle-right MR image is 64-year-old man with ischemic cardiomyopathy; right MR image is 25-year-old woman with hypertrophic cardiomyopathy. LV = left ventricular, SSFP = steady-state free precession.

This article discusses myocardial imaging in ICM and NICM first by outlining the standard sequences used in cardiac MRI and then by highlighting mapping and strain imaging that may add additional diagnostic value and prognostic value. Next, emerging cardiac MRI techniques for myocardial imaging are addressed. Finally, practical approaches for evaluation of myocardial disease with cardiac MRI in specific entities including ischemic heart disease, infiltrative disorders, and genetic cardiomyopathies are described.

Standard Sequences

The typical MRI sequences that are used for the detection and characterization of myocardial disorders can be broadly divided into functional assessment and tissue characterization sequences. Table 1 outlines endpoints derived from each sequence to guide clinical management.

Functional assessment can be performed using cine imaging, typically bSSFP sequences, acquired in standard cardiac planes including at multiple levels in the short-axis plane (Figs. 2A–2D). The blood pool is bright on cine imaging, allowing clear delineation of the blood pool from the myocardium. High temporal resolution is required because images are acquired throughout the cardiac cycle with ECG gating, which allows the identification of end-systole and end-diastole. From cine images, ventricular volumes, mass, and function are calculated. Cine imaging also allows the identification of regional wall motion abnormalities, such as hypokinesis, akinesis, and dyskinesis, and visual inspection of velocity flow jets.

Real-time cine images can be acquired to assess for altered myocardial motion such as in cases of suspected constrictive pericarditis. High-temporal-resolution images are acquired at the mid ventricle to aid in identification of paradoxical septal motion toward the left ventricle during early diastole. This abnormal motion is more evident during inspiration than expiration, and images can be obtained over numerous respiratory cycles.

Multiple different sequences can be acquired for tissue characterization including black blood, T2*, mapping, perfusion, and contrast-enhanced imaging. Black blood imaging can be performed with either T1- or T2-weighting. In black blood sequences, the blood pool is nulled during a double inversion recovery, which allows clear demarcation of the subendocardium. T1-weighted black blood images allow anatomic evaluation including clear depiction of the pericardium. T2-weighted black blood sequences can be performed with or without fat saturation to highlight areas of edema, which can be seen in various clinical entities including acute ischemia, myocarditis, and sarcoidosis [5, 6]. Edema on a T2-weighted sequence can also provide prognostic information after reperfusion in acute ischemia [7].

T2* imaging takes advantage of local magnetic field inhomogeneity that occurs in the presence of paramagnetic materials such as iron. Using gradient-echo sequences with a low flip angle, long TE, and no refocusing pulse, dephasing due to magnetic field inhomogeneity can be detected [8]. When tissues contain paramagnetic material T2*, relaxation occurs faster, as can be seen in both primary and secondary iron overload states [9]. In patients with cardiomyopathy, higher T2* values may also provide prognostic information for risk of adverse cardiac events [10].

First-pass perfusion imaging allows the depiction of contrast distribution in real time. Gradient-echo T1-weighted sequences are performed during the administration of contrast material typically at dedicated levels

TABLE 1: Derived Endpoints From Cardiac MRI Pulse Sequences That Guide Clinical Management

| Sequence	Endpoints	Role in Management
LGE	Presence and type of LGE	Primary endpoint
Cine	Systolic function (ejection fraction)	Secondary endpoint
	Ventricular volume, wall morphology	Other secondary endpoints
T2*	Iron deposition	Secondary endpoint
T1 mapping	Diffuse fibrosis	Exploratory endpoint
T2 mapping	Tissue edema	Exploratory endpoint

Note—LGE = late gadolinium enhancement.
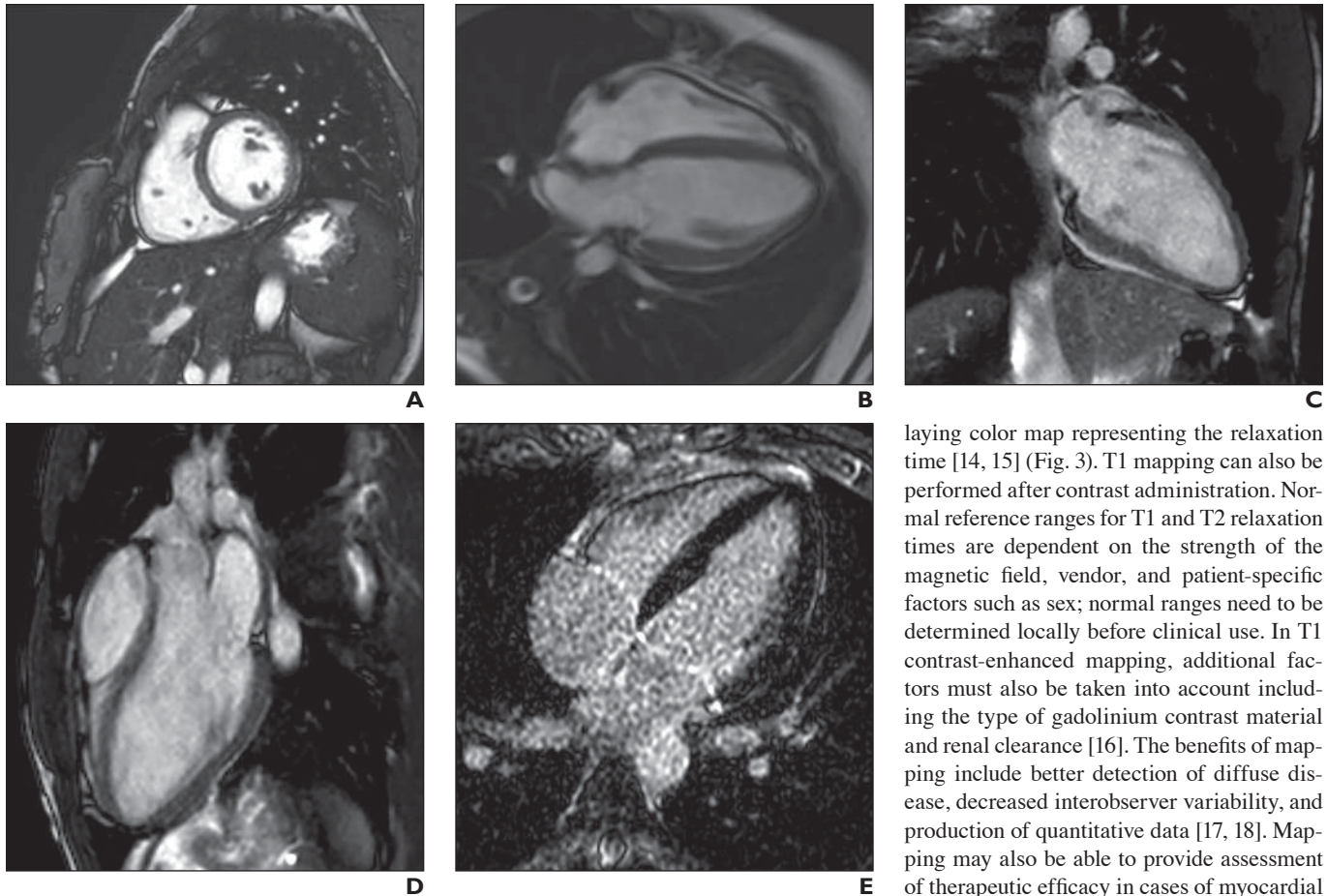
Fig. 2—35-year-old woman with frequent premature ventricular contractions who was referred to undergo cardiac MRI.

A–D, Balanced steady-state free precession MR images are obtained in standard cardiac planes: short-axis (**A**), four-chamber and horizontal long-axis (**B**), two-chamber and vertical long-axis (**C**), and three-chamber (**D**) views. These images allow quantification of ventricular function, volume, and mass; assessment for global and regional wall motion abnormalities; and evaluation of myocardial wall morphology.

E, Late gadolinium enhancement (LGE) MRI is performed 10 minutes after administration of IV gadolinium. On LGE images like this LGE image, areas of fibrosis, edema, and increased extracellular matrix can be identified as white on background of black myocardium, which has been nulled.

(i.e., base, mid ventricle, and apex). Images are quickly obtained over the course of the contrast administration so that areas of myocardium with abnormal perfusion can be identified. Aside from vasodilator myocardial perfusion imaging, which is widely used to diagnose ischemia, perfusion imaging can be useful for identifying microvascular obstruction (as can be seen in postinfarct states) and hyperemia (as can be seen in myocarditis) [11–13].

Of all the cardiac MRI sequences, LGE images play the greatest role in the characterization of cardiomyopathy into ischemic and nonischemic subtypes in addition to providing prognostic information. An inversion recovery gradient sequences nulls the myocardium; hence, the areas of increased extracellular volume (due to fibrosis, edema, or an infiltrative process), which retain gadolinium-based contrast material, can be identified as bright on the background of a black myocardium (Fig. 2E). Typically, images are acquired 10–15 minutes after contrast administration to optimize peak uptake of contrast material in the diseased myocardium.

Additional Sequences

T1 and T2 mapping are newer methods for the detection of myocardial disease using alterations in the native T1 or T2 relaxation of the myocardium. Both T1 and T2 mapping require multiple images to be obtained at various TR or TE times, respectively, to calculate a relaxation curve, which can then be displayed as an absolute value for a given region of the heart or as an image with an over-laying color map representing the relaxation time [14, 15] (Fig. 3). T1 mapping can also be performed after contrast administration. Normal reference ranges for T1 and T2 relaxation times are dependent on the strength of the magnetic field, vendor, and patient-specific factors such as sex; normal ranges need to be determined locally before clinical use. In T1 contrast-enhanced mapping, additional factors must also be taken into account including the type of gadolinium contrast material and renal clearance [16]. The benefits of mapping include better detection of diffuse disease, decreased interobserver variability, and production of quantitative data [17, 18]. Mapping may also be able to provide assessment of therapeutic efficacy in cases of myocardial disease such as sarcoid [19].

Although cine imaging can be used to obtain global cardiac function parameters (e.g., ejection fraction [EF], volumes, and mass), regional myocardial deformation and contractility are obtained from cine imaging, mainly because of the homogeneous myocardial signal intensity in cine images. Although wall motion can be extracted from endo- and epicardial contours in the cine images, intramyocardial tissue motion remains unknown because of the lack of tissue features that can be tracked during the cardiac cycle. Recently, a group of techniques—known as "feature tracking" or "tissue tracking" [20]—have been developed to try to quantify myocardial motion using cine images; these techniques mimic strain imaging from speckle tracking echocardiography. However, in contrast to echo imaging, the cine MR images lack these speckles (or features) and have much lower temporal resolution, which makes MRI feature tracking more accepted for measuring global and integrated motion parameters (e.g., global strain) rather than regional and differential parameters (e.g., strain rate).
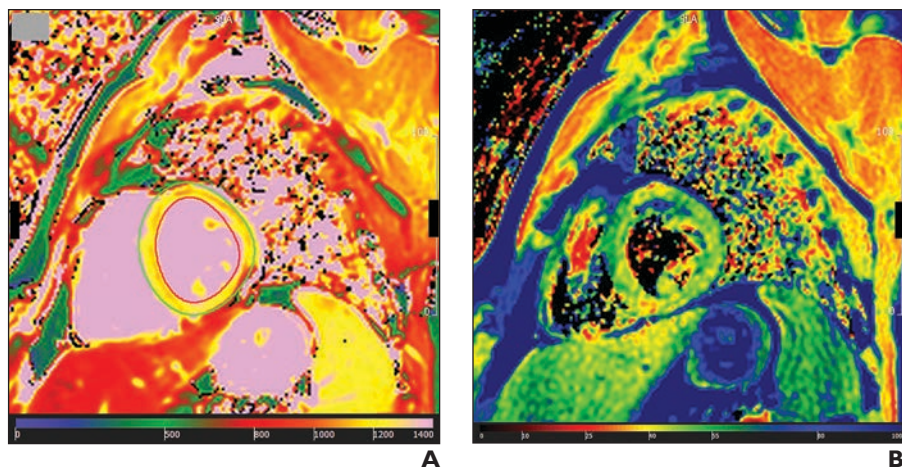
Fig. 3—Normal relaxation times for T1 and T2 in healthy 45-year-old woman.
A and **B**, Color maps show relaxation time for T1 (**A**) and T2 (**B**). Scale shows times in milliseconds. In **A**, red outline shows endocardial border and green outline shows epicardial border.

Nevertheless, there exists a group of established MRI pulse sequences for imaging regional myocardial deformation with great accuracy. These techniques can be broadly categorized into magnitude-based and phase-based techniques in which motion information is encoded into the MRI magnitude and phase images, respectively [21].

The most commonly used tissue-tracking technique is MRI tagging [22]. In MRI tagging, a grid of saturated magnetization is superimposed on the cine magnitude images at the beginning of the cardiac cycle; the grid gets deformed from one time frame to another to reflect myocardium contractility and relaxation during systole and diastole, respectively. MRI tagging allows clear visual inspection of regional myocardial contractility as well as motion quantification. Processing the tagged images can be done directly by tracking the grid-tagged pattern or by analyzing the k-space, similar to harmonic phase analysis [23], in which the latter results in much faster (almost in real time) tagged image analysis.

Strain-encoding (SENC) [24] is another magnitude-based technique. Similar to conventional MRI tagging, SENC is based on applying parallel planes of saturated magnetization into the acquired images; however, in contrast to tagging, these tagged planes lie parallel to and inside the acquired image and therefore through-plane motion (rather than in-plane motion in tagging) is measured by estimating how the tagged planes get closer together or farther apart during the cardiac cycle. Compared with MRI tagging, SENC has the advantages of faster image acquisi-

tion, higher resolution, and simpler post-processing that results in color-coded strain maps. Displacement-encoding with stimulated echoes (DENSE) [25, 26] and tissue phase mapping (TPM) [27] are two pulse sequences in which tissue displacement and velocity, respectively, are encoded into the MRI phase images. These techniques allow quantifying myocardial motion with high sensitivity and in 3D, although this information comes at the cost of a relatively longer scanning time [28].

Myocardial tagging and contractility assessment techniques have been used in several clinical and research studies, which showed these techniques to be valuable for providing detailed information about myocardial motion that complements information from other MRI sequences [28]. These techniques have been used for measuring regional left ventricular (LV) function [29], right ventricular (RV) contractility pattern [30], heart rotation and torsion motion [31], coronary artery disease [32], ischemic heart disease [33], dilated cardiomyopathy [34], hypertrophic cardiomyopathy (HCM) [35], interventricular synchrony [34], valvular diseases [36], congenital heart disease [37], postsurgery cardiac function [38], and other heart diseases [39]. The importance of analyzing myocardial contractility is that regional cardiac function measures (e.g., strain, strain rate, and torsion) have been shown to be affected at early phases of cardiovascular disease development before a reduction in global function (e.g., EF) is observed; detection of cardiovascular disease at early phases allows early intervention, better prognosis, and reduced treatment cost [21].

Emerging Techniques

Multiple new techniques assessing myocardial disease are currently under investigation including ASL, diffusion imaging, and MR spectroscopy. In ASL, water molecules in blood are either saturated or inverted [40]. If the molecules reach the capillary bed, T1 signal is reduced and this reduction is proportional to the blood flow. The images are then standardized to the native T1 signal in which the water molecules are not labeled [41]. ASL allows assessment of perfusion without the use of contrast material, and possible clinical applications include cardiac stress imaging and identification of the area at risk after acute myocardial infarction [42, 43].

The use of DWI has been limited in cardiac imaging because of motion (both respiratory and cardiac) as well as the intrinsic short relaxation time of the myocardium, which requires faster imaging than what is required in neuroimaging [44]. With faster imaging acquisition techniques, DWI is being evaluated in various myocardial disorders including as a contrast material–free method to detect fibrosis and for the depiction of edema [45–47].

MR spectroscopy can assess for various metabolites that can be affected by myocardial disorders. Depending on the metabolite that is to be assessed, a specific radiofrequency energy is applied to detect that metabolite. Triglycerides content, pyruvate metabolism, and phosphocreatine concentration are currently being investigated in imaging of ICM and NICM [48, 49].

A Practical Approach for Evaluating Myocardial Disease

Before image acquisition, a thorough review of the clinical questions, patient history, and prior imaging is crucial. For example, if a clinical history is concerning for iron overload state, T2* imaging should be added. Obtaining and reviewing key sequences and planes on the basis of the clinical concerns are paramount. Figure 4 outlines the interpretation algorithm to diagnosing cardiomyopathy on the basis of pulse sequences and endpoints.

In cases of chronic ischemic heart disease, first the LGE sequence can be assessed for the presence or lack of LGE. Ischemic patterns of enhancement follow a vascular distribution (i.e., territories of the epicardial vessels) and first involve the subendocardium and then progress outward in more severe cases (Fig. 5). Findings on bSSFP images can be correlated with areas of LGE for wall
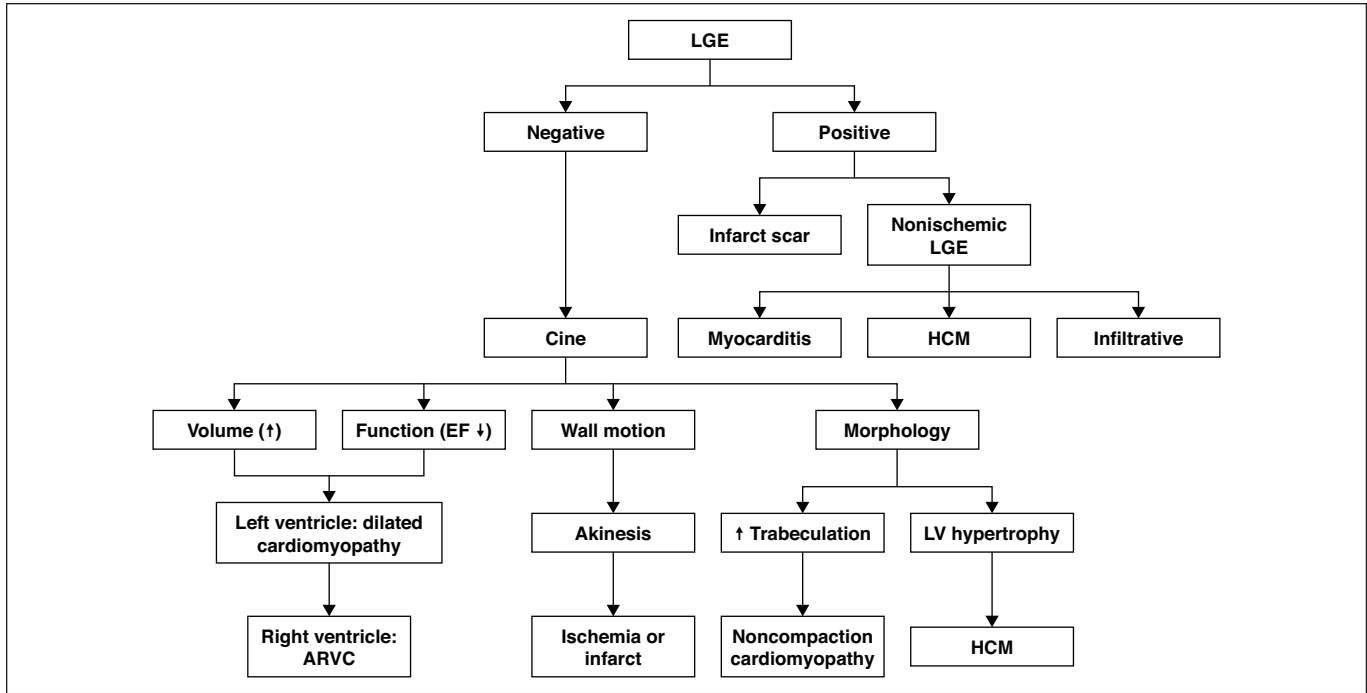
Fig. 4—Interpretation algorithm for diagnosis of cardiomyopathy based on pulse sequences and derived endpoints. Presence and type of late gadolinium enhancement (LGE) are primary endpoint that defines infarct scar versus nonischemic LGE pattern such as global subendocardial LGE seen in cardiac amyloid, patchy LGE in sarcoid, mid wall LGE in myocarditis, and septal patchy LGE in hypertrophic cardiomyopathy (HCM). Secondary endpoints are derived from cine images and include assessment of myocardial wall morphology such as hypertrophy in HCM or hypertensive cardiomyopathy and trabeculations in noncompaction cardiomyopathy. Assessment of myocardial wall morphology is followed by assessment of ventricular function by ejection fraction (EF) and quantification of ventricular volumes. In case of dilated ventricles and depressed EF, diagnosis of left ventricular (LV) dilated cardiomyopathy or arrhythmogenic right ventricular cardiomyopathy (ARVC) can be made. We also assess ventricular volume, function, and mass in patients with positive LGE. Cine images allow evaluation of regional wall motion abnormality, such as hypokinesis, akinesis, and dyskinesis, that can also be seen in ischemia in absence of LGE.

motion abnormalities. If no LGE is present, assessment for regional wall motion abnormalities on bSSFP images can help identify areas of hibernating myocardium that may benefit from revascularization along with areas of LGE involving less than 50% of the myocardial width [50, 51]. The presence of LGE is a poor prognostic sign in these cases, although there is insufficient evidence to change clinical management on the basis of LGE [52]. Cardiac MRI is also being evaluated for its role in acute ischemia and after reperfusion [53–55].

Nonischemic myocardial disorders, in contrast, can cause patterns of LGE that do not follow a vascular territory and can affect any portion of the myocardium without directionality to the progression. A wide variety of pathophysiologic mechanisms in this group of disorders can ultimately lead to impaired cardiac function. Cardiac MRI sequences used in the evaluation of these disorders are tailored to the specific entity that is clinically suspected or known.
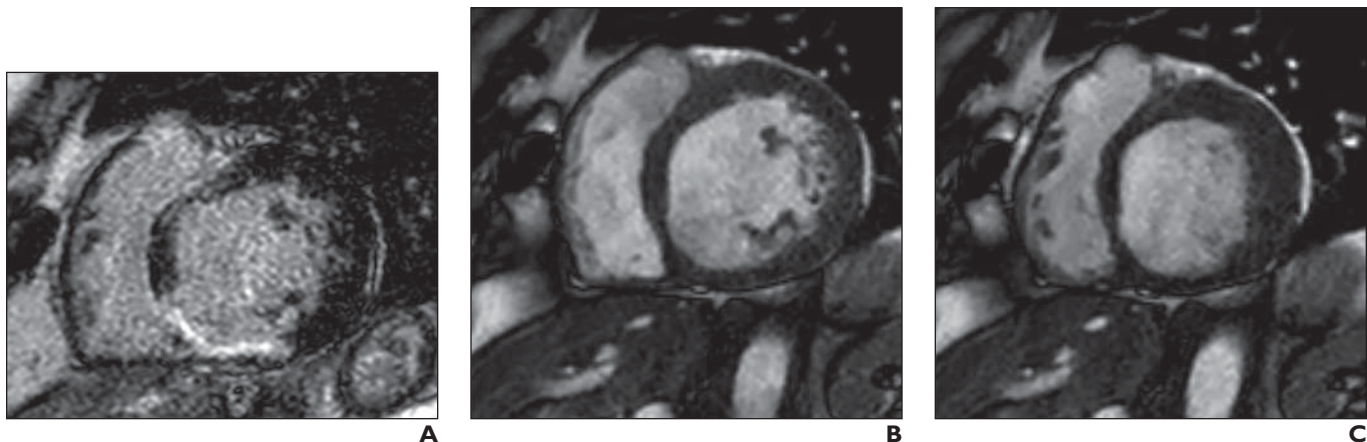
Fig. 5—64-year-old man with ischemic cardiomyopathy who was referred to cardiac MRI for evaluation of cardiac viability.
A, Short-axis late gadolinium-enhanced MR image shows extensive transmural enhancement in right coronary artery distribution.
B and **C,** Diastole (**B**) and systole (**C**) steady-state free precession MR images show akinesis. This area of myocardium is considered nonviable and would likely not benefit from revascularization.

Fig. 6—Two cases of infiltrative cardiomyopathy.
A, 72-year-old man with multiple myeloma referred to undergo cardiac MRI to evaluate for cardiac amyloidosis. Four-chamber late gadolinium-enhanced MR image shows thickening of myocardial walls and extensive subendocardial enhancement of left ventricle as well as atria.
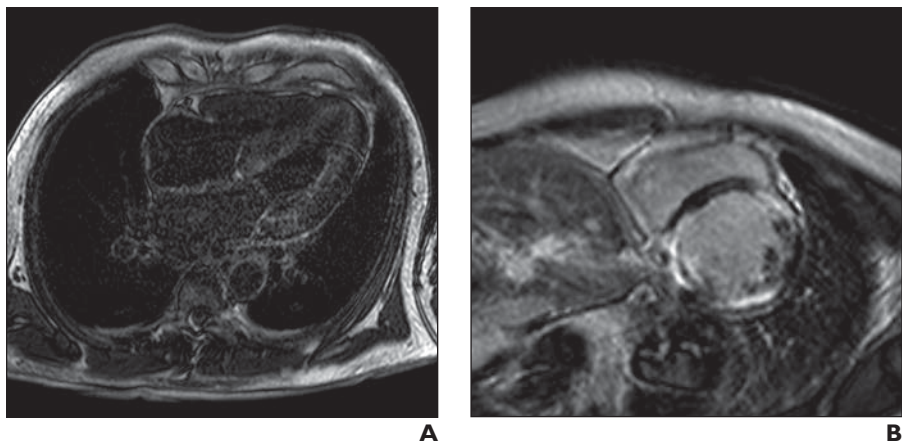**B,** 44-year-old man referred to undergo cardiac MRI for evaluation of cardiac sarcoid. Short-axis late gadolinium-enhanced MR image shows patchy, nodular midmyocardial late gadolinium enhancement pattern, which is consistent with sarcoid.

Infiltrative myocardial disorders include amyloidosis, sarcoid, and iron deposition disorders (i.e., primary or secondary hemochromatosis). Amyloidosis results in altered signal intensity on multiple sequences because of the deposition of proteins in the extracellular space of the myocardium [56]. The abnormal protein alters the T1 of the myocardium, leading to difficulty with nulling the myocardium and to increased T1 relaxation, which can be measured with mapping [57, 58]. T2 signal is also altered with a decreased ratio of myocardial-to–skeletal muscle T2 signal intensity seen in amyloidosis [59]. LGE sequences can be used to identify patterns of enhancement consistent with amyloidosis, including subendocardial, transmural, or midmyocardial, that occur in a nonvascular distribution (Fig. 6A). Sensitivity and specificity of MRI for the detection of amyloid using LGE are reported to be more than 86% [60]. MRI can allow the noninvasive diagnosis of cardiac amyloidosis, which is especially critical because novel drug therapies for the transthyretin form of amyloid have been developed [61].

Cardiac sarcoidosis is also considered an infiltrative cardiomyopathy. Societal recommendation for imaging cardiac sarcoid includes acquisition of bSSFP, LGE, and T2-weighted sequences, and evidence for the use of mapping is still evolving [62]. Cardiac MRI is sensitive for the diagnosis of cardiac sarcoid; however, imaging findings alone on MRI cannot make the diagnosis because of a low specificity [63, 64]. T2 signal may be increased in areas of active inflammation. LGE patterns of enhancement that have been described in sarcoid include transmural and subendocardial; however, the most commonly reported pattern is midmyocardial enhancement or subepicardial enhancement involving the lateral or septal basal segments [65] (Fig. 6B). The presence of LGE indicates a risk for arrhythmias and adverse cardiac events [66].

For quantification of iron deposition, T2* images are obtained to measure the relaxation constant of the myocardium. Because of the paramagnetic effects of iron, T2* time is decreased in iron overload states. T2* times of less than 10 milliseconds indicate a high risk of developing heart failure and that chelation therapy is required, whereas T2* times of greater than 20 milliseconds indicate a low risk [67] (Fig. 7). Serial cardiac MRI can be used to monitor response to therapy [68] in cases of cardiac hemochromatosis. T2* time is best measured in the interventricular septum because the septum most accurately reflects myocardial iron levels [69].

Multiple additional nonischemic, noninfiltrative causes of myocardial disease exist. Diabetic cardiomyopathy occurs in patients without evidence of cardiovascular disease and is hypothesized to occur as a consequence of inflammation, oxidative stress, and impaired myocyte metabolism in the setting of altered glucose and insulin metabolism. Early in the disease course, LV hypertrophy is present with normal systolic function on bSSFP images, whereas in later phases of the disease, a systolic dysfunction can occur [70, 71]. There is growing evidence that changes to the myocardium in these patients can be quantified using advanced techniques including T1 mapping and MR spectroscopy [72, 73].

Both hypertensive cardiomyopathy and HCM lead to abnormal thickening of the ventricular wall. In hypertension, cardiomyopathy-increased afterload can result in an increase in overall LV mass or an increase in wall thickness, which can be measured using bSSFP images. These findings are of prognostic significance, and stricter blood pressure control may be warranted when present [74]. Hypertrophy is typically symmetric, and
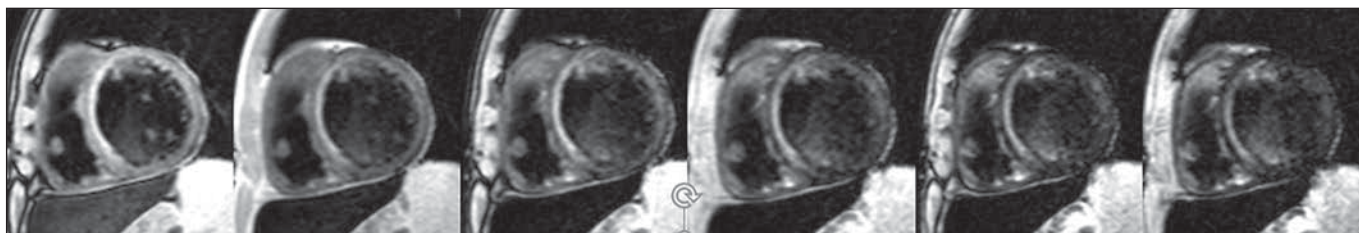
Fig. 7—45-year-old woman with thalassemia who had received multiple transfusions and was referred to cardiac MRI to evaluate for iron deposition. Short-axis MR images obtained at level of midventricle with different TEs; TE times increase from left to right, with left image showing shortest TE and right image showing longest TE. When T2* times are less than 10 milliseconds, as in this patient with sideroblastic anemia, chelation therapy is warranted because of high risk for development of heart failure.

Fig. 8—25-year-old woman with history of hypertrophic cardiomyopathy (HCM).
A, Contrast-enhanced short-axis MR image shows mid myocardial wall enhancement in anterior and inferior septum.
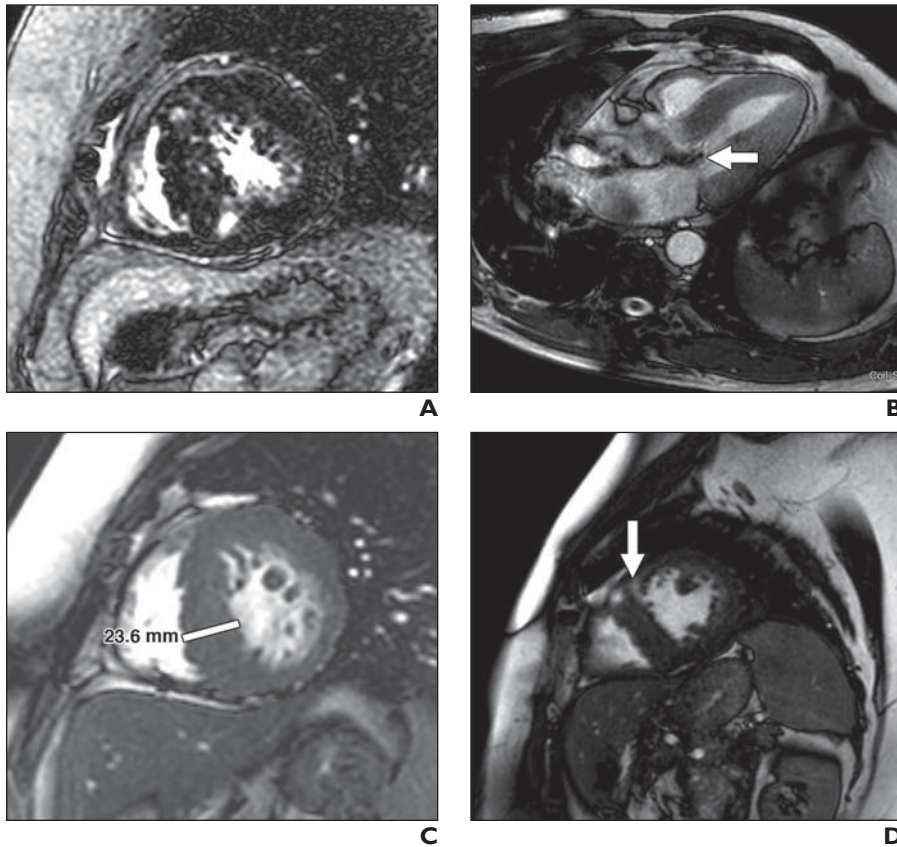**B,** Three-chamber balanced steady-state free precession (bSSFP) MR image. Dephasing jet (*arrow*) due to flow turbulence can be seen in left ventricular outflow tract.
C and **D,** Short-axis bSSFP MR images show additional findings associated with HCM diagnosis including wall thickness of more than 15 mm (*line*, **C**), regional bulging of left ventricular wall, abnormalities involving mitral valve apparatus, and myocardial crypts (*arrow*, **D**).

Fig. 9—62-year-old woman with nonischemic cardiomyopathy of unclear cause referred to undergo cardiac MRI to evaluate for scar. Short-axis balanced steady-state free precession MR image shows alterations in ratio of noncompacted to compacted myocardium.

LGE may or may not be present; when present, LGE is typically not subendocardial and can have a variable appearance [75]. Differentiation of hypertensive cardiomyopathy from HCM may be difficult especially in older patients when asymmetric septal hypertrophy is present. When LV wall thickness is greater than 15 mm or is 12–14 mm in a patient with the appropriate family history, HCM should be considered as the leading diagnosis. One caveat here is that in patients with long-standing, undertreated hypertension, particularly those with chronic kidney disease or with end-stage renal disease, moderate to severe concentric LV hypertrophy is not rare.

Additional findings to support HCM as a diagnosis including maximal wall thickness involving the anterior wall, regional bulging of the LV wall, abnormalities involving the mitral valve apparatus, and myocardial crypts, all of which can be identified on bSSFP images [76, 77]. The bSSFP images allow better quantification of maximal wall thickness in cases of HCM than echocardiography and may provide additional information when assessing the need for primary preventive therapy with cardiovascular implanted electronic devices (CIEDs) [78]; bSSFP images can also allow the diagnosis of LV outflow obstruction and systolic anterior motion of the mitral valve (Fig. 8). On LGE sequences, patchy globular septal enhancement is more commonly seen in HCM than in hypertensive cardiomyopathy [79]. In patients with HCM, LGE involving more than 15% of the myocardium indicates that the patient may benefit from CIED placement for primary prevention [80]. Advanced techniques for differentiation of HCM from hypertensive cardiomyopathy include strain imaging, which shows increased wall stress in hypertensive cardiomyopathy and reduced longitudinal strain in HCM [81]. There is also emerging evidence about the use of T1 map-
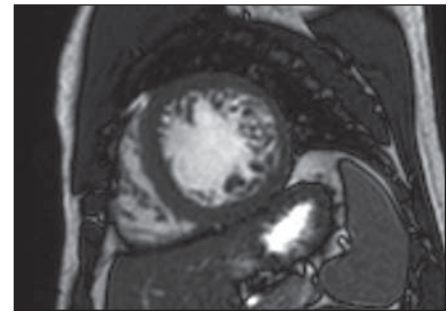
ping for discrimination between HCM and hypertensive cardiomyopathy [82].

In cases of suspected noncompaction cardiomyopathy, bSSFP images allow assessment for and quantification of the ratio of noncompacted to compacted myocardium; the diagnostic criteria for noncompaction cardiomyopathy include a ratio of noncompacted to compacted myocardium of greater than 2.3 on the long-axis view (Fig. 9). Additional diagnostic criteria are published with varying degrees of sensitivity using steady-state free precession images for evaluation [83, 84]. The presence of LGE and the presence of LV dilatation are poor prognostic signs [85]. Fibrosis measured by T1 mapping may be present even when LGE is not [86]. Strain imaging may also be impaired and may allow discrimination of noncompaction cardiomyopathy from dilated cardiomyopathy: strain imaging of patients with noncompaction cardiomyopathy shows higher longitudinal and radial strain than strain imaging of patients with dilated cardiomyopathy [87].

A large spectrum of pathophysiologic mechanisms can lead to dilated cardiomyopathy including genetic abnormalities, infections, and toxins. This wide spectrum of conditions ultimately leads to a decrease in systolic function and enlargement of either the left ventricle or both ventricles; bSSFP images allow quantification of the degree of dilatation as well as the degree to which the EF is depressed. LGE sequences show fibrosis, and the pattern of enhancement may be helpful in determining the cause and may provide prognostic information. Patients with septal or free wall LGE experience higher rates of adverse cardiac events than those showing other LGE patterns [88, 89]. There is emerging evidence for the use
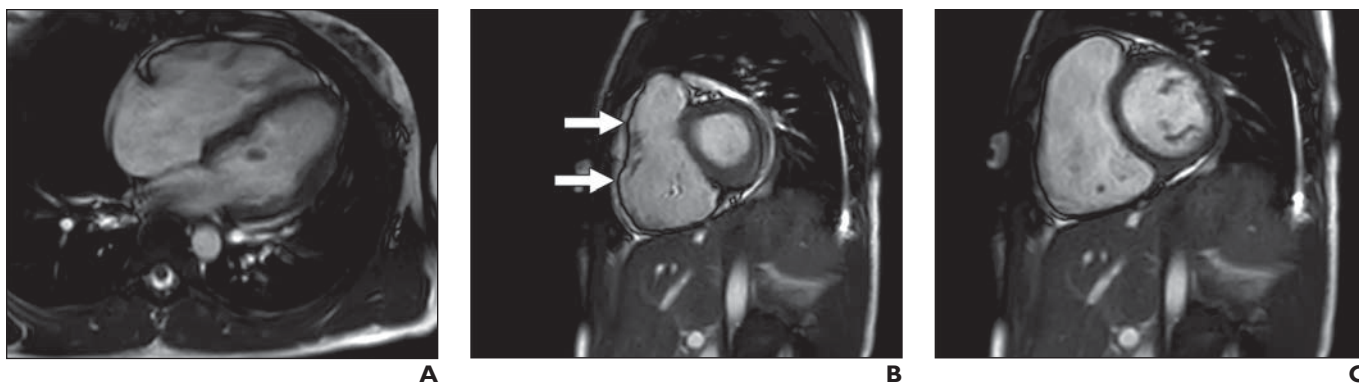
Fig. 10—16-year-old girl who presented with cardiac arrhythmia. Diagnostic criteria for arrhythmogenic right ventricular cardiomyopathy (ARVC) rely on identifying abnormalities on balanced steady-state free precession (bSSFP) MR images.
A, Four-chamber bSSFP image shows dilatation of right ventricle and decreased systolic function, which are abnormalities that are included in diagnostic criteria for ARVC.
B and **C,** Short-axis bSSFP images show major diagnostic criteria for ARVC including presence of regional wall motion abnormality along anterior wall (*arrows*, **B**) during systole.

of T1 mapping in these patients as a method to identify extracellular matrix expansion [90, 91].

In patients with suspected arrhythmogenic right ventricular cardiomyopathy (ARVC), cardiac MRI plays a contributory role in diagnosis by identification of RV dilatation, impaired RV function, and regional wall motion abnormalities based on bSSFP images [92, 93]. Additional imaging planes, including the two-chamber right ventricle and RV outflow tract views, lead to better assessment of RV regional motion abnormalities, which are pathognomonic findings in cases of ARVC (Fig. 10). LGE can contribute to identifying areas of fibrosis; however, LGE is not part of the task force criteria because of the overlap with other conditions, such as myocarditis, and because identifying LGE may be difficult given the thin RV wall [94, 95]. Strain imaging may improve detection of ARVC substrate [96].

Imaging for myocarditis requires the acquisition of T2-weighted, perfusion, and LGE sequences. For the diagnosis of myocarditis, the Lake Louise criteria can be applied [97]. A regional or global increase in T2 indicating edema, hyperemia represented by increased perfusion, and LGE in a nonvascular distribution indicating inflammation are imaging findings of myocarditis; when two of these three findings are present, the sensitivity for MRI in the diagnosis of myocarditis is 67% and specificity is 91% [97]. Of these imaging findings, LGE is the most sensitive finding in isolation; however, LGE is less specific than perfusion or T2 abnormalities [98]. There is developing evidence for the application of mapping in these patients, and this technique could add value to the Lake Louise criteria [99, 100].

Conclusion

Imaging of myocardial disorders encompasses a large variety of conditions including both ischemic and nonischemic diseases. Cardiac MRI sequences, such as bSSFP and LGE, play a critical role in establishing diagnosis, determining prognosis, and guiding therapeutic management. Additional sequences—including perfusion imaging, T2*, real-time cine, and T2-weighted sequences—should be performed in specific clinical scenarios. There is emerging evidence for the use of mapping in imaging of myocardial disease. Multiple other new techniques are currently being studied. These novel techniques will likely change the way myocardial disorders are understood and diagnosed in the near future.

References

1. Gutberlet M, Noeske R, Schwinge K, Freyhardt P, Felix R, Niendorf T. Comprehensive cardiac magnetic resonance imaging at 3.0 Tesla: feasibility and implications for clinical applications. *Invest Radiol* 2006; 41:154–167
2. Michaely HJ, Nael K, Schoenberg SO, et al. Analysis of cardiac function: comparison between 1.5 Tesla and 3.0 Tesla cardiac cine magnetic resonance imaging—preliminary experience. *Invest Radiol* 2006; 41:133–140
3. Rajiah P, Bolen MA. Cardiovascular MR imaging at 3 T: opportunities, challenges, and solutions. *RadioGraphics* 2014; 34:1612–1635
4. Bhatti L, Hoang JK, Dale BM, Bashir MR. Advanced magnetic resonance techniques: 3 T. *Radiol Clin North Am* 2015; 53:441–455
5. Amano Y, Tachi M, Tani H, Mizuno K, Kobayashi Y, Kumita S. T2-weighted cardiac magnetic resonance imaging of edema in myocardial diseases. *ScientificWorldJournal* 2012; 2012:194069
6. Mirakhur A, Anca N, Mikami Y, Merchant N. T2-weighted imaging of the heart: a pictorial review. *Eur J Radiol* 2013; 82:1755–1762
7. Tada Y, Yang PC. Myocardial edema on T2-weighted MRI: new marker of ischemia reperfusion injury and adverse myocardial remodeling. *Circ Res* 2017; 121:326–328
8. Lota AS, Gatehouse PD, Mohiaddin RH. T2 mapping and T2* imaging in heart failure. *Heart Fail Rev* 2017; 22:431–440
9. Carpenter JP, He T, Kirk P, et al. On T2* magnetic resonance and cardiac iron. *Circulation* 2011; 123:1519–1528
10. Nagao M, Baba S, Yonezawa M, et al. Prediction of adverse cardiac events in dilated cardiomyopathy using cardiac T2* MRI and MIBG scintigraphy. *Int J Cardiovasc Imaging* 2015; 31:399–407
11. Yun CH, Tsai JP, Tsai CT, et al. Qualitative and semi-quantitative evaluation of myocardium perfusion with 3 T stress cardiac MRI. *BMC Cardiovasc Disord* 2015; 15:164
12. Mather AN, Lockie T, Nagel E, et al. Appearance of microvascular obstruction on high resolution first-pass perfusion, early and late gadolinium enhancement CMR in patients with acute myocardial infarction. *J Cardiovasc Magn Reson* 2009; 11:33
13. Vincenti G, Masci PG, Monney P, et al. Stress perfusion CMR in patients with known and suspected CAD: prognostic value and optimal ischemic threshold for revascularization. *JACC Cardiovasc Imaging* 2017; 10:526–537

14. Baxa J, Ferda J, Hromádka M. T1 mapping of the ischemic myocardium: review of potential clinical use. *Eur J Radiol* 2016; 85:1922–1928

15. Montant P, Sigovan M, Revel D, Douek P. MR imaging assessment of myocardial edema with T2 mapping. *Diagn Interv Imaging* 2015; 96:885–890

16. Puntmann VO, Peker E, Chandrashekhar Y, Nagel E. T1 mapping in characterizing myocardial disease: a comprehensive review. *Circ Res* 2016; 119:277–299

17. Hamlin SA, Henry TS, Little BP, Lerakis S, Stillman AE. Mapping the future of cardiac MR imaging: case-based review of T1 and T2 mapping techniques. *RadioGraphics* 2014; 34:1594–1611

18. Mavrogeni S, Apostolou D, Argyriou P, et al. T1 and T2 mapping in cardiology: "mapping the obscure object of desire." *Cardiology* 2017; 138:207–217

19. Puntmann VO, Isted A, Hinojar R, Foote L, Carr-White G, Nagel E. T1 and T2 mapping in recognition of early cardiac involvement in systemic sarcoidosis. *Radiology* 2017; 285:63–72

20. Maret E, Todt T, Brudin L, et al. Functional measurements based on feature tracking of cine magnetic resonance images identify left ventricular segments with myocardial scar. *Cardiovasc Ultrasound* 2009; 7:53

21. Ibrahim ES. *Heart mechanics: magnetic resonance imaging.* Boca Raton, FL: CRC Press, 2017

22. Fischer SE, McKinnon GC, Maier SE, Boesiger P. Improved myocardial tagging contrast. *Magn Reson Med* 1993; 30:191–200

23. Osman NF, Kerwin WS, McVeigh ER, Prince JL. Cardiac motion tracking using CINE harmonic phase (HARP) magnetic resonance imaging. *Magn Reson Med* 1999; 42:1048–1060

24. Osman NF, Sampath S, Atalar E, Prince JL. Imaging longitudinal cardiac strain on short-axis images using strain-encoded MRI. *Magn Reson Med* 2001; 46:324–334

25. Aletras AH, Balaban RS, Wen H. High-resolution strain analysis of the human heart with fast-DENSE. *J Magn Reson* 1999; 140:41–57

26. Epstein FH, Gilson WD. Displacement-encoded cardiac MRI using cosine and sine modulation to eliminate (CANSEL) artifact-generating echoes. *Magn Reson Med* 2004; 52:774–781

27. Jung B, Föll D, Böttler P, Petersen S, Hennig J, Markl M. Detailed analysis of myocardial motion in volunteers and patients using high-temporal-resolution MR tissue phase mapping. *J Magn Reson Imaging* 2006; 24:1033–1039

28. Ibrahim el-SH. Myocardial tagging by cardiovascular magnetic resonance: evolution of techniques: pulse sequences, analysis algorithms, and applications. *J Cardiovasc Magn Reson* 2011; 13:36

29. Clarysse P, Basset C, Khouas L, et al. Two-dimensional spatial and temporal displacement and deformation field fitting from cardiac magnetic resonance tagging. *Med Image Anal* 2000; 4:253–268

30. Haber I, Metaxas DN, Axel L. Three-dimensional motion reconstruction and analysis of the right ventricle using tagged MRI. *Med Image Anal* 2000; 4:335–355

31. Dong SJ, Hees PS, Siu CO, Weiss JL, Shapiro EP. MRI assessment of LV relaxation by untwisting rate: a new isovolumic phase measure of tau. *Am J Physiol Heart Circ Physiol* 2001; 281:H2002–H2009

32. Castillo E, Osman NF, Rosen BD, et al. Quantitative assessment of regional myocardial function with MR-tagging in a multi-center study: interobserver and intraobserver agreement of fast strain analysis with Harmonic Phase (HARP) MRI. *J Cardiovasc Magn Reson* 2005; 7:783–791

33. Kraitchman DL, Sampath S, Castillo E, et al. Quantitative ischemia detection during cardiac magnetic resonance stress testing by use of fast-HARP. *Circulation* 2003; 107:2025–2030

34. Curry CW, Nelson GS, Wyman BT, et al. Mechanical dyssynchrony in dilated cardiomyopathy with intraventricular conduction delay as depicted by 3D tagged magnetic resonance imaging. *Circulation* 2000; 101:E2

35. Ennis DB, Epstein FH, Kellman P, Fananapazir L, McVeigh ER, Arai AE. Assessment of regional systolic and diastolic dysfunction in familial hypertrophic cardiomyopathy using MR tagging. *Magn Reson Med* 2003; 50:638–642

36. Sandstede JJ, Johnson T, Harre K, et al. Cardiac systolic rotation and contraction before and after valve replacement for aortic stenosis: a myocardial tagging study using MR imaging. *AJR* 2002; 178:953–958

37. Fogel MA, Weinberg PM, Gupta KB, et al. Mechanics of the single left ventricle: a study in ventricular-ventricular interaction II. *Circulation* 1998; 98:330–338

38. Pusca SV, Pilla JJ, Blom AS, et al. Assessment of synchronized direct mechanical ventricular actuation in a canine model of left ventricular dysfunction. *ASAIO J* 2000; 46:756–760

39. Fernandes VR, Polak JF, Cheng S, et al. Arterial stiffness is associated with regional ventricular systolic and diastolic dysfunction: the Multi-Ethnic Study of Atherosclerosis. *Arterioscler Thromb Vasc Biol* 2008; 28:194–201

40. Telischak NA, Detre JA, Zaharchuk G. Arterial spin labeling MRI: clinical applications in the brain. *J Magn Reson Imaging* 2015; 41:1165–1180

41. Waller C, Hiller KH, Voll S, Haase A, Ertl G, Bauer WR. Myocardial perfusion imaging using a non-contrast agent MR imaging technique. *Int J Cardiovasc Imaging* 2001; 17:123–132

42. Yoon AJ, Do HP, Cen S, et al. Assessment of segmental myocardial blood flow and myocardial perfusion reserve by adenosine-stress myocardial arterial spin labeling perfusion imaging. *J Magn Reson Imaging* 2017; 46:413–420

43. Dongworth RK, Campbell-Washburn AE, Cabrera-Fuentes HA, et al. Quantifying the area-at-risk of myocardial infarction in-vivo using arterial spin labeling cardiac magnetic resonance. *Sci Rep* 2017; 7:2271

44. Mekkaoui C, Reese TG, Jackowski MP, Bhat H, Sosnovik DE. Diffusion MRI in the heart. *NMR Biomed* 2017; 30:30

45. Aliotta E, Moulin K, Zhang Z, Ennis DB. Simultaneous measurement of T_2 and apparent diffusion coefficient (T_2 + ADC) in the heart with motion-compensated spin echo diffusion-weighted imaging. *Magn Reson Med* 2018; 79:654–662

46. Wu R, An DA, Shi RY, et al. Myocardial fibrosis evaluated by diffusion-weighted imaging and its relationship to 3D contractile function in patients with hypertrophic cardiomyopathy. *J Magn Reson Imaging* 2018; 48:1139–1146

47. An DA, Chen BH, Rui-Wu, et al. Diagnostic performance of intravoxel incoherent motion diffusion-weighted imaging in the assessment of the dynamic status of myocardial perfusion. *J Magn Reson Imaging* 2018; 48:1602–1609

48. Bizino MB, Hammer S, Lamb HJ. Metabolic imaging of the human heart: clinical application of magnetic resonance spectroscopy. *Heart* 2014; 100:881–890

49. Apps A, Lau J, Peterzan M, Neubauer S, Tyler D, Rider O. Hyperpolarised magnetic resonance for in vivo real-time metabolic imaging. *Heart* 2018; 104:1484–1491

50. Sawlani RN, Collins JD. Cardiac MRI and ischemic heart disease: role in diagnosis and risk stratification. *Curr Atheroscler Rep* 2016; 18:23

51. François CJ. Current state of the art cardiovascular MR imaging techniques for assessment of ischemic heart disease. *Radiol Clin North Am* 2015; 53:335–344

52. Kwon DH, Obuchowski NA, Marwick TH, et al. Jeopardized myocardium defined by late gadolinium enhancement magnetic resonance imaging predicts survival in patients with ischemic cardiomyopathy: impact of revascularization. *J Am Heart Assoc* 2018; 7:e009394

53. Kandler D, Lücke C, Grothoff M, et al. The relation between hypointense core, microvascular obstruction and intramyocardial haemorrhage in acute reperfused myocardial infarction assessed by cardiac magnetic resonance imaging. *Eur Radiol* 2014; 24:3277–3288

54. Hammer-Hansen S, Ugander M, Hsu LY, et al. Distinction of salvaged and infarcted myocardium within the ischaemic area-at-risk with T2 mapping. *Eur Heart J Cardiovasc Imaging* 2014; 15:1048–1053

55. Tahir E, Sinn M, Bohnen S, et al. Acute versus chronic myocardial infarction: diagnostic accuracy of quantitative native T1 and T2 mapping versus assessment of edema on standard T2-weighted cardiovascular MR images for differentiation. *Radiology* 2017; 285:83–91

56. Fontana M, Banypersad SM, Treibel TA, et al. Differential myocyte responses in patients with cardiac transthyretin amyloidosis and light-chain amyloidosis: a cardiac MR imaging study. *Radiology* 2015; 277:388–397

57. Lee SP, Park JB, Kim HK, Kim YJ, Grogan M, Sohn DW. Contemporary imaging diagnosis of cardiac amyloidosis. *J Cardiovasc Imaging* 2019; 27:1–10

58. Wan K, Li W, Sun J, et al. Regional amyloid distribution and impact on mortality in light-chain amyloidosis: a t1 mapping cardiac magnetic resonance study. *Amyloid* 2019; 26:45–51

59. Legou F, Tacher V, Damy T, et al. Usefulness of T2 ratio in the diagnosis and prognosis of cardiac amyloidosis using cardiac MR imaging. *Diagn Interv Imaging* 2017; 98:125–132

60. Rigopoulos AG, Ali M, Abate E, et al. Advances in the diagnosis and treatment of transthyretin amyloidosis with cardiac involvement. *Heart Fail Rev* 2019; 24:521–533

61. Harikrishnan P, Yandrapalli S, Aronow WS, Lanier GM, Jain D. Novel drug therapies for cardiac amyloidosis. *Expert Opin Investig Drugs* 2019; 28:497–499

62. Writing group; Document reading group; EACVI Reviewers: This document was reviewed by members of the EACVI Scientific Documents Committee for 2014–2016 and 2016–2018. A joint procedural position statement on imaging in cardiac sarcoidosis: from the Cardiovascular and Inflammation & Infection Committees of the European Association of Nuclear Medicine, the European Association of Cardiovascular Imaging, and the American Society of Nuclear Cardiology. *Eur Heart J Cardiovasc Imaging* 2017; 18:1073–1089

63. Divakaran S, Stewart GC, Lakdawala NK, et al. Diagnostic accuracy of advanced imaging in cardiac sarcoidosis. *Circ Cardiovasc Imaging* 2019; 12:e008975

64. Zhang J, Li Y, Xu Q, Xu B, Wang H. Cardiac magnetic resonance imaging for diagnosis of cardiac sarcoidosis: a meta-analysis. *Can Respir J* 2018; 2018:7457369

65. Patel MR, Cawley PJ, Heitner JF, et al. Detection of myocardial damage in patients with sarcoid-osis. *Circulation* 2009; 120:1969–1977

66. Tan JL, Fong HK, Birati EY, Han Y. Cardiac sarcoidosis. *Am J Cardiol* 2019; 123:513–522

67. Aronow WS. Management of cardiac hemochromatosis. *Arch Med Sci* 2018; 14:560–568

68. Wood JC. Guidelines for quantifying iron overload. *Hematology Am Soc Hematol Educ Program* 2014; 2014:210–215

69. Chu WC, Au WY, Lam WW. MRI of cardiac iron overload. *J Magn Reson Imaging* 2012; 36:1052–1059

70. Asghar O, Al-Sunni A, Khavandi K, et al. Diabetic cardiomyopathy. *Clin Sci (Lond)* 2009; 116:741–760

71. Paolillo S, Marsico F, Prastaro M, et al. Diabetic cardiomyopathy: definition, diagnosis, and therapeutic implications. *Heart Fail Clin* 2019; 15:341–347

72. Mordi IR. Non-invasive imaging in diabetic cardiomyopathy. *J Cardiovasc Dev Dis* 2019; 6:6

73. Gao Y, Yang ZG, Ren Y, et al. Evaluation of myocardial fibrosis in diabetes with cardiac magnetic resonance T1-mapping: correlation with the high-level hemoglobin A1c. *Diabetes Res Clin Pract* 2019; 150:72–80

74. Janardhanan R, Kramer CM. Imaging in hypertensive heart disease. *Expert Rev Cardiovasc Ther* 2011; 9:199–209

75. Giesbrandt KJ, Bolan CW, Shapiro BP, Edwards WD, Mergo PJ. Diffuse diseases of the myocardium: MRI-pathologic review of nondilated cardiomyopathies. *AJR* 2013; 200:[web]W266–W273

76. Bogaert J, Olivotto I. MR imaging in hypertrophic cardiomyopathy: from magnet to bedside. *Radiology* 2014; 273:329–348

77. Urbano-Moral JA, Gutierrez-Garcia-Moreno L, Rodriguez-Palomares JF, et al. Structural abnormalities in hypertrophic cardiomyopathy beyond left ventricular hypertrophy by multimodality imaging evaluation. *Echocardiography* 2019; 36:1241–1252

78. Sanaani A, Fuisz A. Cardiac magnetic resonance for diagnosis and risk stratification. *Cardiol Clin* 2019; 37:27–33

79. Rodrigues JC, Rohan S, Ghosh Dastidar A, et al. Hypertensive heart disease versus hypertrophic cardiomyopathy: multi-parametric cardiovascular magnetic resonance discriminators when end-diastolic wall thickness ≥ 15 mm. *Eur Radiol* 2017; 27:1125–1135

80. Moore B, Semsarian C, Chan KH, Sy RW. Sudden cardiac death and ventricular arrhythmias in hypertrophic cardiomyopathy. *Heart Lung Circ* 2019; 28:146–154

81. Puntmann VO, Jahnke C, Gebker R, et al. Usefulness of magnetic resonance imaging to distinguish hypertensive and hypertrophic cardiomy-opathy. *Am J Cardiol* 2010; 106:1016–1022

82. Neisius U, El-Rewaidy H, Nakamori S, Rodriguez J, Manning WJ, Nezafat R. Radiomic analysis of myocardial native T_1 imaging discriminates between hypertensive heart disease and hypertrophic cardiomyopathy. *JACC Cardiovasc Imaging* 2019; 12:1946–1954

83. Di Fusco SA, Lucà F, Madeo A, et al. Left ventricular noncompaction: diagnostic approach, prognostic evaluation, and management strategies. *Cardiol Rev* 2019 Apr 12 [Epub ahead of print]

84. Ivanov A, Dabiesingh DS, Bhumireddy GP, et al. Prevalence and prognostic significance of left ventricular noncompaction in patients referred for cardiac magnetic resonance imaging. *Circ Cardiovasc Imaging* 2017; 10:e006174

85. Andreini D, Pontone G, Bogaert J, et al. Long-term prognostic value of cardiac magnetic resonance in left ventricle noncompaction: a prospective multicenter study. *J Am Coll Cardiol* 2016; 68:2166–2181

86. Araujo-Filho JA, Assuncao AN Jr, Tavares de Melo MD, et al. Myocardial T1 mapping and extracellular volume quantification in patients with left ventricular non-compaction cardiomyopathy. *Eur Heart J Cardiovasc Imaging* 2018; 19:888–895

87. Zheng T, Ma X, Li S, et al. Value of cardiac magnetic resonance fractal analysis combined with myocardial strain in discriminating isolated left ventricular noncompaction and dilated cardiomyopathy. *J Magn Reson Imaging* 2019; 50:153–163

88. Halliday BP, Baksi AJ, Gulati A, et al. Outcome in dilated cardiomyopathy related to the extent, location, and pattern of late gadolinium enhancement. *JACC Cardiovasc Imaging* 2019; 12(8 Pt 2):1645–1655

89. Sree Raman K, Nucifora G, Leong DP, et al. Long term prognostic importance of late gadolinium enhancement in first-presentation non-ischaemic dilated cardiomyopathy. *Int J Cardiol* 2019; 280:124–129

90. Cui Y, Chen Y, Cao Y, et al. Myocardial extracellular volume fraction measurements with MOLLI 5(3)3 by cardiovascular MRI for the discrimination of healthy volunteers from dilated and hypertrophic cardiomyopathy patients. *Clin Radiol* 2019; 74:732.e9–732.e16

91. Vita T, Grani C, Abbasi SA, et al. Comparing CMR mapping methods and myocardial patterns toward heart failure outcomes in nonischemic dilated cardiomyopathy. *JACC Cardiovasc Imaging* 2019; 12(8 Pt 2):1659–1669

92. Marcus FI, McKenna WJ, Sherrill D, et al. Diagnosis of arrhythmogenic right ventricular cardiomyopathy/dysplasia: proposed modification of the Task Force Criteria. *Eur Heart J* 2010; 31:806–814

93. Amadu AM, Baritussio A, Dastidar AG, et al. Arrhythmogenic right ventricular cardiomyopathy (ARVC) mimics: the knot unravelled by cardiovascular MRI. *Clin Radiol* 2019; 74:228–234

94. Gandjbakhch E, Redheuil A, Pousset F, Charron P, Frank R. Clinical diagnosis, imaging, and genetics of arrhythmogenic right ventricular cardiomyopathy/dysplasia: JACC state-of-the-art review. *J Am Coll Cardiol* 2018; 72:784–804

95. Oomen AW, Semsarian C, Puranik R, Sy RW. Diagnosis of arrhythmogenic right ventricular cardiomyopathy: progress and pitfalls. *Heart Lung Circ* 2018; 27:1310–1317

96. Zghaib T, Ghasabeh MA, Assis FR, et al. Regional strain by cardiac magnetic resonance imaging improves detection of right ventricular scar compared with late gadolinium enhancement on a multimodality scar evaluation in patients with arrhythmogenic right ventricular cardiomyopathy. *Circ Cardiovasc Imaging* 2018; 11:e007546

97. Gannon MP, Schaub E, Grines CL, Saba SG. State of the art: evaluation and prognostication of myocarditis using cardiac MRI. *J Magn Reson Imaging* 2019; 49:e122–e131

98. Wei S, Fu J, Chen L, Yu S. Performance of cardiac magnetic resonance imaging for diagnosis of myocarditis compared with endomyocardial biopsy: a meta-analysis. *Med Sci Monit* 2017; 23:3687–3696

99. Lurz P, Luecke C, Eitel I, et al. Comprehensive cardiac magnetic resonance imaging in patients with suspected myocarditis: the MyoRacer-Trial. *J Am Coll Cardiol* 2016; 67:1800–1811

100. Huber AT, Bravetti M, Lamy J, et al. Non-invasive differentiation of idiopathic inflammatory myopathy with cardiac involvement from acute viral myocarditis using cardiovascular magnetic resonance imaging T1 and T2 mapping. *J Cardiovasc Magn Reson* 2018; 20:11